Polymer Journal (2017) 49, 825–830

www.nature.com/pj

ORIGINAL ARTICLE

Polymer-assisted shapeable synthesis of porous frameworks consisting of silica nanoparticles with mechanical property tuning

Kanako Sato[1], Kanji Ishii[1], Yuya Oaki[1], Kazuki Nakanishi[2] and Hiroaki Imai[1]

We report the shapeable synthesis of porous silica frameworks using polyacrylamide (PAAm) gel as an organic template and hydrolyzed silicon alkoxide as a silica source. Macroscopically shaped porous frameworks—such as plates, tablets and sheets—comprised of 20- to 40-nm diameter silica particles are obtained via PAAm–silica precursor gels. The mechanical properties (i.e., hardness and Young's modulus) of the silica frameworks depend on the packing density and are controlled by changing the silica content in PAAm gels.
Polymer Journal (2017) **49,** 825–830; doi:10.1038/pj.2017.62; published online 11 October 2017

INTRODUCTION

Amorphous silica, an industrially important inorganic polymer, is an essential biomineral produced by organisms. Biogenic silicas (*biosilicas*) are widely observed in nature, for example, diatom frustules,[1–6] sponge spicules[7–13] and silicified cells in some higher plants.[14–21] These biosilicas are known to provide excellent mechanical properties. For instance, the silica frustules of diatoms, which have a honeycomb sandwich plate architecture and a low flow density, demonstrate an unprecedented high specific strength.[6] Sponge spicules consisting of mainly hydrated silica cylinders separated by a thin organic layer are much tougher, both in bending and tension, than synthetic silica glass.[7,8] Our recent research has revealed that two main types of biosilicas (*plant opals*) in rice plants (*Oryza sativa L.*) (i.e., silica plates and fan-shaped silica) consist of nanoparticles 10 to 100 nm in diameter and display different mechanical properties that depend on nanoparticles' packing states; silica plates that comprised of loosely packed nanoparticles demonstrate high flexibility, whereas fan-shaped silicas that comprised of tightly packed nanoparticles are rigid.[22] The mechanics of biosilicas consisting of nanoparticles can be designed by changing the packing of the nanoparticles. Thus, the ability of biosilicas to express altered properties by controlling their hierarchical structures and their ambient synthesis process provides insights into the design of functional and environmentally friendly silica glass.

The hierarchically organized biosilicas were reported to be synthesized using organic molecules, such as silaffin,[4,5,23] silicatein[13,24,25] and long-chain polyamines[26,27] under ambient conditions. In rice plants, silicon is taken up by the roots in the form of silicic acid and is deposited on cell walls as a polymer of hydrated amorphous silica.[18] In studies on the biomimetic synthesis of silica, the interaction between amino groups in organic molecules such as polyamines and silica sources (i.e., silicic acid derivatives) is considered to promote biosilicification.[5,23] In previous works, polyamines have been shown to catalyze the polycondensation of silanol groups[28] and to act as efficient flocculation agents.[29] Zhou *et al.*[30] and Pi *et al.*[31] reported that nano- and submicrometer-sized porous, core shell and hollow silica particles were synthesized using polyamines as a colloidal template. In addition, our previous work showed that silicates accumulated on a long-chain branched polyethylenimine and then transformed to bunching nanoparticles similar to biosilica in rice plants.[32] Thus, numerous studies have recently demonstrated the biomimetic synthesis of nanoscale silicas (i.e., nanoparticles, hollow spheres and fibers) using polyamines. However, the sophisticated architectures of amorphous silica with controlled morphologies and mechanical properties (i.e., porous silica frameworks like plant opals) have not been produced using polyamines.

Many kinds of porous silica frameworks were obtained by conventional sol-gel methods. For instance, ordered hexagonal mesoporous silica structures with uniform pore sizes were obtained by using amphiphilic triblock copolymers to direct the organization of polymerizing silica species.[33] The formation of three-dimensional mesoporous silica structures patterned over multiple length scales was achieved by the assembly of an inorganic sol-gel-block copolymer mesophase around an organized array of latex spheres in patterned molds.[34] A well-defined macroporous silica structure and several variations of tailoring mesoporous structures within the macroporous silica were obtained by inducing a phase separation parallel to the sol-gel transition of alkoxy-derived silica systems.[35,36] Hollow porous silica microspheres were synthesized using freeze dried

[1]Department of Applied Chemistry, Faculty of Science and Technology, Keio University, Yokohama, Japan and [2]Department of Chemistry, Graduate School of Science, Kyoto University, Kyoto, Japan
Correspondence: Professor H Imai, Department of Applied Chemistry, Faculty of Science and Technology, Keio University, 3-14-1 Hiyoshi, Kohoku-ku, Yokohama 223-8522, Japan.
E-mail: hiroaki@applc.keio.ac.jp
Received 20 July 2017; revised 22 August 2017; accepted 23 August 2017; published online 11 October 2017

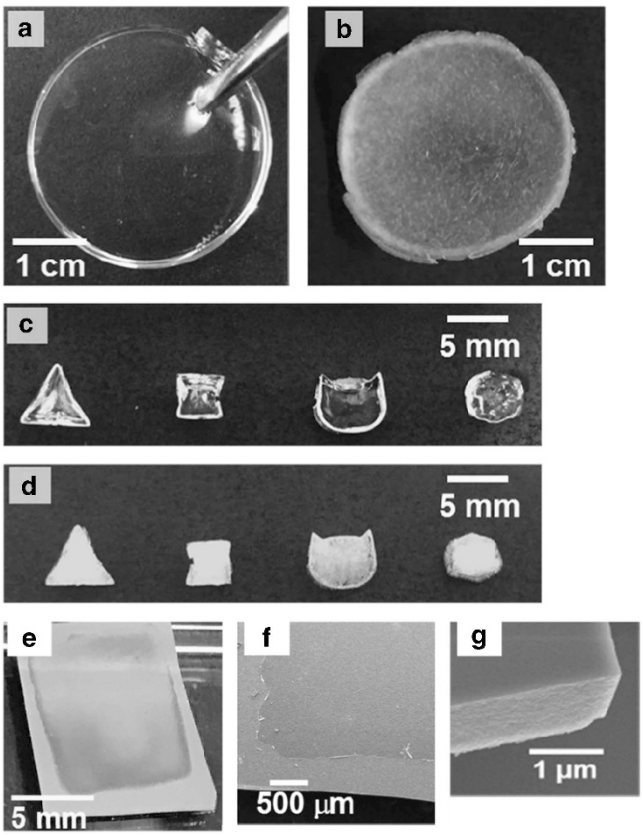

Figure 1 Photographs of dried precursor gels ([Si]/[AAm] = 1.0) (**a**, **c**) and the resultant products after calcination (**b**, **d**); a photograph (**e**) and SEM images (**f**, **g**) of thin plates on a silicon substrate after calcination ([Si]/[AAm] = 0.1 (**e**, **f**) and 1.0 (**g**)).

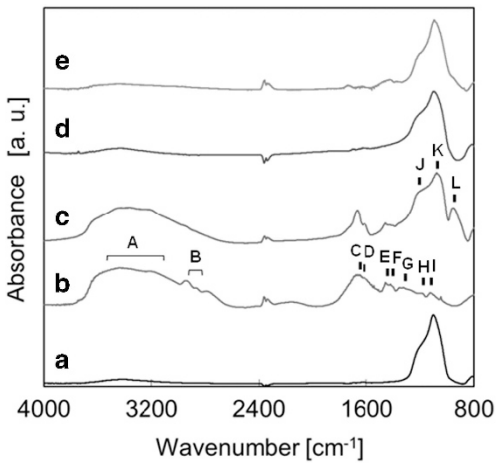

Figure 2 FT–IR spectra of fused silica (**a**), pure PAAm gel (**b**), PAAm – silica precursor gel ([Si]/[AAm] = 1.0) (**c**), white products after calcination (**d**), and plant opals in a rice plant after calcination at 300°C in air for 3 h (**e**). (A) stretching vibration of N–H groups, (B) stretching vibration of $–CH_2$, (C) stretching vibration of the C = O groups of amide, (D) deformation vibrations of $–NH_2$ groups, (E) deformation vibrations of $–CH_2$, (F, H) deformation vibrations of –NH groups, (G) stretching vibrations of –NH groups, (I) C–N or N–H bonds, (J, K) stretching vibration of Si–O–Si bonds, and (L) stretching vibration of Si–OH bonds.

polyacrylamide (PAAm) microgels as the substrates on which the polycondensation reaction of silicon alkoxide occurred.[37] However, porous frameworks comprised of silica nanoparticles that control their macroscopic shape and mechanical properties have not been studied.

In the present work, we report the polymer-assisted shapeable synthesis of porous silica frameworks consisting of nanoparticles similar to the nanostructure of plant opals in rice plants. Here, we tuned the mechanical properties of the silica frameworks that were obtained after the calcination of PAAm –silica precursor gel. Since PAAm contains many amide groups and has a strong hydrogen-bonding effect, PAAm is expected to exert a mutually beneficial influence on silicate species in place of polyamines. In alcohol-based systems, homogeneous composites of silica and polymers were produced by *in situ* polymerization methods.[38,39] As the polycondensation reactions of acrylamide (AAm) monomers and silicates occur sequentially in a water-based system, porous silica frameworks that consist of nanoparticles are produced in the polymer matrix. Moreover, we succeeded in controlling both the macroscopic shape and the nanostructures of silica frameworks as well as their mechanical properties.

EXPERIMENTAL PROCEDURES

Synthesis of silica in PAAm gels

(a) Preparation of an aqueous solution containing AAm monomer and hydrolyzed silicon alkoxide. A monomer aqueous solution was prepared by dissolving 1.00 g of AAm (Kanto Chemical, Tokyo, Japan), 0.02 g of *N*, *N*′-methylenebisacrylamide (Kanto Chemical) as a cross-linker and 0.12 g of ammonium persulfate (Kanto Chemical) as a polymerization initiator in 4.5 cm^3 of pure water, followed by stirring for 0.5 h at room temperature. A hydrolyzed silicon alkoxide solution was prepared by mixing 26.8 cm^3 of tetraethyl orthosilicate (Tokyo Chemical, Tokyo, Japan) and 8.29 cm^3 of pure water whose pH was adjusted to 2.0 by adding concentrated hydrochloric acid (Kanto Chemical), followed by stirring for 1.5–2.0 h at room temperature. The molar ratio of tetraethyl orthosilicate and pure water was 1:4 in the silicic solution. The clear, colorless solution of an AAm monomer and hydrolyzed silicon alkoxide was prepared by adding 0.43–12.9 cm^3 of the silicic solution into a certain amount of the AAm monomer solution. The molar ratio of [Si]/[AAm] in the mixed solutions ranged from 0.1 to 3.0 were prepared. The schematic illustration of the experimental procedure is shown in Supplementary Figure S1a.

(b) Polymerization of PAAm and hydrolyzed silicon alkoxide. PAAm–SiO_2 precursor gels (Figures 1a and c) were produced by placing the mixed solutions in a Petri dish and subsequent drying at 60 °C for 24 h. The polymerization of AAm occurred in 0.5–1.0 h, and the dehydration and polycondensation of hydrolyzed silicon alkoxide flocculated on PAAm networks by the hydrogen-bonding effect were then induced. The macroscopic morphology of the precursor gels was shaped by using molds of glass and silicone resin. Thin plates were produced by dropping of the precursor solution on a silicon substrate, sandwiching by another silicon plate and subsequent polymerization. The porous silica frameworks having macroscopic shapes that inherited those of the dried precursor gels (Figures 1b and d) were obtained after the removal of PAAm by calcination at 600 °C in air for 3 h. Hence, PAAm gels acted as a template for the porous silica framework in this synthesis system. The schematic illustration of the experimental procedure is shown in Supplementary Figure S1b.

Characterization

The chemical structures of PAAm–silica precursor gels and the resultant porous silica frameworks after calcination were analyzed using Fourier transform infrared absorption with the KBr method. The silica content in the precursor gels was investigated by thermogravimetry (Seiko TG-DTA 6200 Instruments, Chiba, Japan). The morphology of the silica frameworks was investigated using field-emission scanning electron microscopy (SEM) (Hitachi S-4700 (Tokyo, Japan), FEI-SIRON (Hillsboro, OR, USA), JEOL JSM-7600F, Tokyo, Japan). The pore-size distributions of the silica frameworks were investigated using mercury porosimetry (Micromeritics AutoPore IV 9500, Norcross, GA, USA)

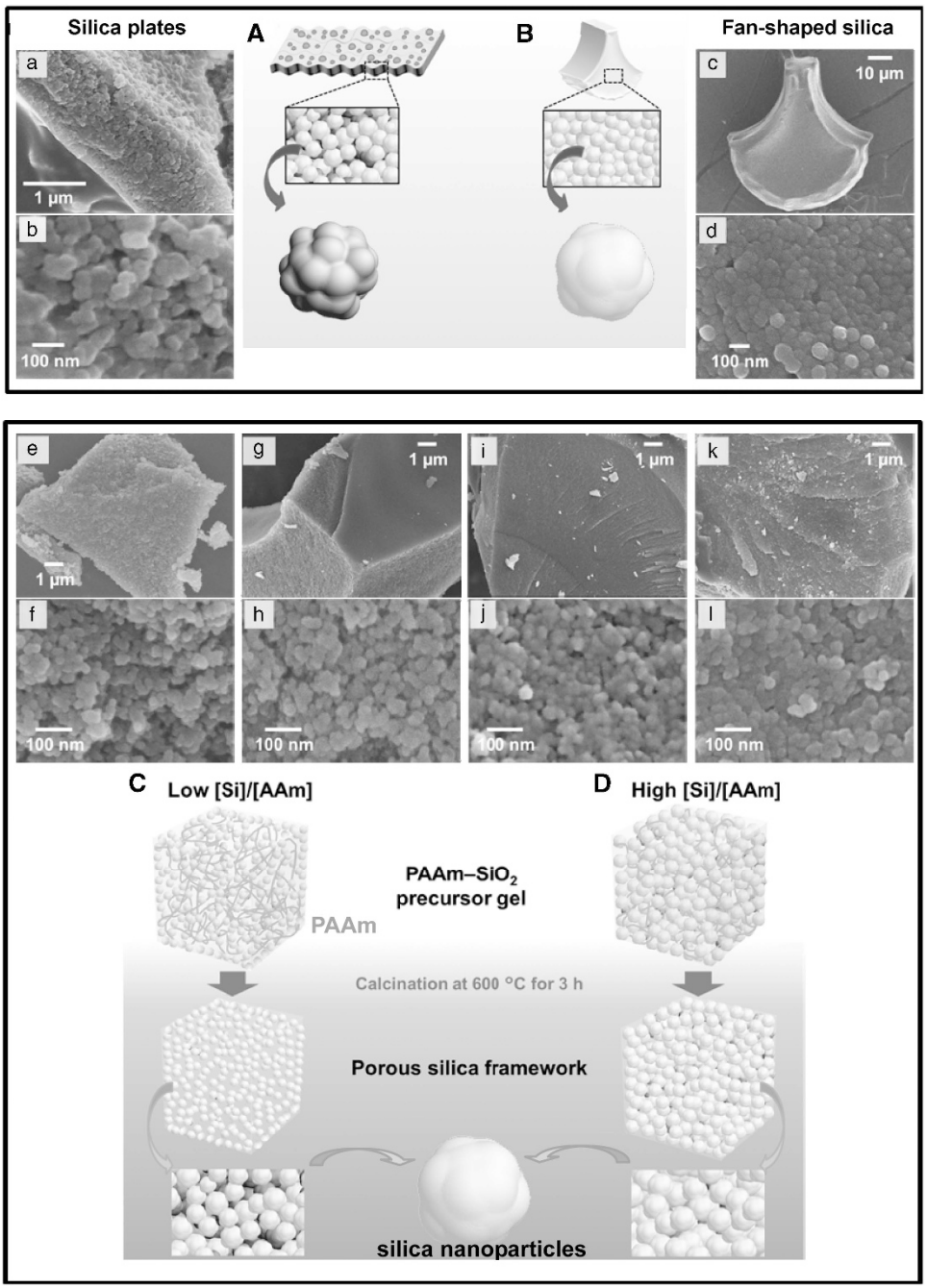

Figure 3 SEM micrographs of silica plates (**a**, **b**) and fan-shaped silicas (**c**, **d**) in a rice plant after calcination at 300°C in air for 3 h,[22] and fragments of the products obtained after the calcination of PAAm – SiO_2 precursor gels (**e** – **l**). The molar ratio of Si/AAm ([Si]/[AAm]) of the precursor gel was 0.1 (**e**, **f**), 0.3 (**g**, **h**), 1.0 (**i**, **j**), and 3.0 (**k**, **l**). Schematic illustrations of plant opals (A: silica plate, B: fan-shaped silica), PAAm – SiO_2 precursor gels and silica frameworks of low (C) and high [Si]/[AAm] (D). Silica particles are comprised of primary particles (5 – 10 nm). Smaller secondary particles (26.4 ± 6.1 nm) are loosely packed in low [Si]/[AAm] and larger secondary particles (33.6 ± 5.8 nm) are tightly packed in high [Si]/[AAm]. A full color version of this figure is available at *Polymer Journal* online.

and the nitrogen sorption method (Micromeritics 3Flex-3M, Norcross, GA, USA). The hardness and Young's modulus of the silica frameworks embedded in epoxy resin were investigated using a dynamic ultramicro hardness tester (Shimadzu DUH-211, Kyoto, Japan) furnished with a Berkovich diamond tip. The resin blocks were polished using a polisher on a 1000 grit silicon carbide paper, and then additional polishing was performed to produce smoother surfaces using 1.0–0.1 μm polycrystalline alumina suspensions. Polished samples were indented by 10 mN to evaluate the hardness and Young's modulus from load-displacement curves using the Oliver–Pherr method.[40]

RESULTS AND DISCUSSION

Silica formation via PAAm–silica precursor gels

Clear and colorless precursor gels (Figures 1a and c) were obtained after AAm and hydrolyzed silicon alkoxide were polymerized and

subsequently dried at 60 °C. The macroscopic morphology of the gels was shaped by using molds of glass and silicone resin (Figures 1a and c). Based on thermogravimetry analysis (Supplementary Figure S2), the silica content in the precursor gels was consistent with the raw material ratio (i.e., [Si]/[AAm] = 0.1 etc.).

The structures of precursor gels and the resultant products were characterized by Fourier transform infrared absorption spectra. Figure 2 shows the Fourier transform infrared absorption spectra of fused silica (a), pure PAAm gel (b), precursor gels before calcination (c), white products after calcination (d) and plant opal in a rice plant after calcination (e). The bands assigned to N–H and C–H bonds, the C = O groups of amide, $–NH_2$ groups, $–CH_2$ groups and –NH groups are present in the spectrum of pure PAAm gel (Figure 1b). The bands assigned to Si–O–Si bonds and Si–OH bonds are observed in the spectra of both fused silica and plant opals in a rice plant (Figures 1a and e). In the spectrum of the PAAm–silica precursor gel (Figure 1c), several absorption bands due to Si–O–Si and Si–OH bonds of silica appear at 1200, 1050 and 950 cm^{-1}, in addition to absorption bands assigned to the chemical bonds in PAAm. Therefore, an Si–O–Si network similar to that of artificial silica was formed in a complex with PAAm in the precursor gel. According to the spectrum of the calcined products (Figure 2d), pure silica was obtained by removing the organic molecules from precursor gels at 600 °C after 3 h. After PAAm was removed by calcination, translucent white inorganic bodies that inherited the shapes of the dried PAAm–silica precursor gel were obtained (Figures 1b and d). Thin plates ~ 1 μm thick were obtained from a film of PAAm–silica precursor gel sandwiched between two silicon plates (Figures 1e–g). We successfully controlled the macroscopic shape of silica via PAAm–silica precursor gels and obtained bulky plates, tablets and thin films. It is generally difficult to fabricate bulky bodies as shown in Figure 1 using conventional sol-gel methods because of the formation of many cracks during the drying and calcination processes. The drying process is very important for the preparation of bulky products using a mold through the conventional sol-gel methods. On the other hand, the drying conditions, such as temperature and volume of vessels, are not essential for the fabrication of molded products using this polymer-assisted method. The presence of PAAm prevents the formation of cracks and deformation of the products. In the present polymer-assisted method, we easily obtain various bulky shapes of silica without cracks through a simple process.

Table 1 Cumulative pore volumes of the silica frameworks and plant opals after calcination at 300 °C in air for 3 h[22] evaluated using mercury porosimetry and relative density estimated from pore volumes

Sample		*Pore volume*[a] *($cm^3\ g^{-1}$)*	*Relative density*
[Si]/[AAm]	0.1	1.63	0.22
	0.3	1.35	0.25
	1.0	1.18	0.28
	3.0	0.44	0.51
Silica plate	0.71	0.39	
Fan-shaped silica	0.36	0.56	

Abbreviations: AAm, acrylamide.
[a]The total volume of closed pores and open pores smaller than 200 nm estimated by mercury porosimetry.

Nanostructures of biomimetic porous silica

Figure 3 shows SEM images of plant opals in a rice plant[22] and the products obtained after the calcination of PAAm–silica precursor gels, whose molar ratio of Si/AAm (i.e., [Si]/[AAm]) ranged between 0.1 and 3.0. Based on SEM observations, we found that the calcined products were comprised of particles 10–50 nm in diameter and had porous structures (Figures 3e–l) that were similar to those of plant opals in a rice plant (Figures 3a–d). Hence, we succeeded in synthesizing frameworks that consisted of silica nanoparticles similar to those of plant opals as illustrated in Figures 3a–d. As is the case of plant opals produced by biosilicification in organic matrices (i.e., plant cells), we could obtain silica architectures with nanostructures similar to those of plant opals in a rice plant using organic templates.

In Figures 3e–l, the packing states of nanoparticles of the silica framework depend on [Si]/[AAm] in the precursor gels. To

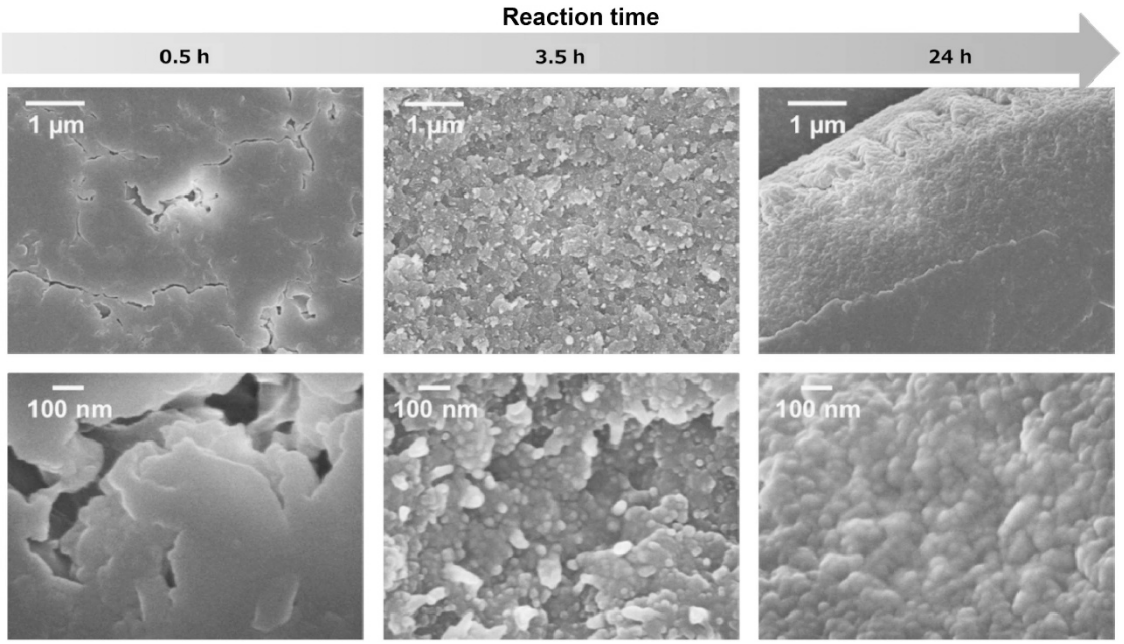

Figure 4 SEM micrographs of the fractured surface of PAAm – SiO_2 precursor gels ([Si]/[AAm] = 1.0) dried after various reaction times.

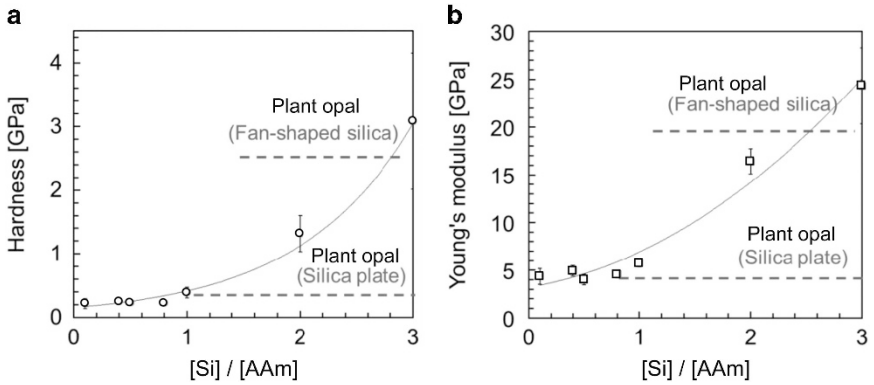

Figure 5 Hardness (**a**) and Young's modulus (**b**) as a function of [Si]/[AAm] of the silica frameworks.

quantitatively evaluate their porous structures, we explored the pore volumes of the silica frameworks. As shown in SEM images (Figures 3b, d, f, h, j and l), the porous structures are characterized by the volume of pores smaller than 200 nm. Hence, we evaluated the volume of closed pores and open pores smaller than 200 nm in the silica frameworks using mercury porosimetry. Table 1 shows the pore volumes and the relative density of the silica frameworks and plant opals. To estimate the relative density of silica frameworks, we assumed that the density of the silica matrix is the same as that of silica glass, 2.2 g cm^{-3}. The relative density of the silica frameworks increases with the silica content in the precursor gels. We successfully produced porous frameworks consisting of silica nanoparticles similar to plant opals by changing the molar ratio. Precursor gels with a high PAAm content ([Si]/[AAm] = 0.1 and 0.3) were more swollen with water than were those with a high silica content ([Si]/[AAm] = 3.0). Therefore, silica frameworks from dried precursor gels with a low silica content tend to contain larger volumes of pores than do those from precursor gels with high silica contents. We show schematic illustrations that summarize the silica frameworks in Figures 3c and d.

To characterize the detailed nanostructures of porous silica frameworks, we estimated the Brunauer–Emmett–Teller-specific surface areas using the nitrogen adsorption method (Supplementary Figure S3). The Brunauer–Emmett–Teller-specific surface areas of silica frameworks were 250–500 m^2 g^{-1}. The specific surface areas decreased with increasing [Si]/[AAm]. The diameters of the silica particles as building blocks of the silica frameworks were calculated from the specific surface area. The calculated diameters, ca. 5–10 nm, were smaller than the particle size shown in Figure 3. This indicates that the 20–40-nm particles observed in the silica frameworks (Figures 3f, h, j and l) consist of primary particles 5–10 nm in size.

The process of forming silica frameworks

The process of forming silica frameworks was monitored by SEM images of the fractured surface of PAAm–SiO_2 precursor gels as shown in Figure 4. Gelation was completed within 0.5 h under conditions used in the present study. However, we observed no grains in the homogeneous matrix that had submicron-scale cracks. The grains 20–30 nm in size, appeared 3.5 and 24 h after the reaction started. This indicates that the AAm monomer initially polymerized and the polymer network was then produced with hydrolyzed silicon precursors. Then, silica particles were formed in the polymer matrix.

Mechanical properties of silica frameworks

The hardness and Young's modulus of silica frameworks were evaluated via indentation experiments. As shown in Figure 5, both the hardness and Young's modulus of the silica frameworks increased with increasing [Si]/[AAm]. The variation of the mechanical properties covers those of plant opals in a rice plant.[22] As mentioned in a previous work,[41] the Young's modulus of a synthesized amorphous silica increases with increasing relative density (Supplementary Figure S4). As discussed in the structural characterization, the relative density of the silica frameworks increased with increasing [Si]/[AAm]. The hardness and Young's modulus were confirmed to correlate with the relative density (Supplementary Figure S5). Thus, we successfully tuned the mechanical properties of porous silica frameworks by changing the [Si]/[AAm]. In the present work, we succeeded in producing silica frameworks that were well controlled in both nanostructures and mechanical properties similar to those of plant opals in rice plants.

CONCLUSION

We successfully synthesized porous frameworks that consist of silica nanoparticles via PAAm–silica precursor gels. The macroscopic morphology and relative density of silica frameworks were controlled by using molds and changing the silica content in the precursor gels, respectively. The mechanical properties of the silica frameworks were dependent on the relative density, which was tuned by the silica content in the precursor gels. This polymer-assisted synthesis of structurally and mechanically controlled silica frameworks provides insights into the future design of porous silica. Moreover, the hierarchical structures, packing density and mechanical properties of the artificial silicas are similar to those of biogenic silicas in a rice plant. Basically, the silica frameworks are produced in the polymer matrix at room temperature. These results suggest that the specific silica structures of plant opals are formed with the assistance of organic polymeric molecules.

CONFLICT OF INTEREST

The authors declare no conflict of interest.

ACKNOWLEDGEMENTS

We gratefully acknowledge assistance for sample preparation by S Funyu and mercury prosimetry measurements by Dr Kei Morisato at the Kyoto University/GL Sciences. This work was supported by Grant-in-Aid for Scientific Research (A) (16H02398) from Japan Society for the Promotion of Science.

1 Coradin, T. & Lopez, P. J. Biogenic silica patterning: Simple chemistry or subtle biology? *ChemBioChem* **4**, 251–259 (2003).
2 Foo, C. W., Huang, J. & Kaplan, D. L. Lessons from seashells: silica mineralization via protein templating. *Trends Biotechnol.* **22**, 577–585 (2004).

3 Gordon, R., Losic, D., Tiffany, M. A., Nagy, S. S. & Sterrenburg, F. A. S. The Glass Menagerie: diatoms for novel applications in nanotechnology. *Trends Biotechnol.* **27**, 116–127 (2008).
4 Kröger, K. & Poulsen, N. Diatoms—from cell wall biogenesis to nanotechnology. *Annu. Rev. Genet.* **42**, 83–107 (2008).
5 Hildebrand, M. Diatoms, biomineralization processes, and genomics. *Chem. Rev.* **108**, 4855–4874 (2008).
6 Aitken, Z. H., Luo, S., Reynolds, S. N., Thaulow, C. & Greer, J. R. Microstructure provides insights into evolutionary design and resilience of *Coscinodiscus* sp. frustule. *Proc. Natl Acad. Sci. USA* **113**, 2017–2022 (2016).
7 Weaver, J. C., Milliron, G. W., Allen, P., Miserez, A., Rawal, A., Garay, J. P., Thurner, J., Seto, J., Mayzel, B., Friesen, L., Chmelka, J. B. F., Fratzl, P., Aizenberg, J., Dauphin, Y., Kisailus, D. & Morse, D, E. Unifying design strategies in Demosponge and Hexactinellid skeletal systems. *J. Adhes.* **86**, 72–95 (2010).
8 Müller, W. E. G., Wang, X., Kropf, K., Ushijima, H., Geurtsen, W., Eckert, C., Tahir, M. N., Tremel, W., Boreiko, A., Schloßmacher, U., Li, J. & Schröder, H. C. Bioorganic/inorganic hybrid composition of sponge spicules: matrix of the giant spicules and of the comitalia of the deep sea hexactinellid Monorhaphis. *J. Struct. Biol.* **161**, 188–203 (2008).
9 Aizenberg, J., Sundar, V. C., Yablon, A. D., Weaver, J. C. & Chen, G. Biological glass fibers: Correlation between optical and structural properties. *Proc. Natl Acad. Sci. USA* **101**, 3358–3363 (2004).
10 Aizenberg, J., Weaver, J. C., Thanawala, M. S., Sundar, V. C., Morse, D. E. & Fratzl, P. Skeleton of *Euplectella* sp.: structural hierarchy from the nanoscale to the macroscale. *Science* **309**, 275–278 (2005).
11 Müller, W. E. G., Wang, X., Sinha, B., Wiens, M., Schröder, H. C. & Jochum, K. P. NanoSIMS: insights into the organization of the proteinaceous scaffold within Hexactinellid sponge spicules. *ChemBioChem* **11**, 1077–1082 (2010).
12 Müller, W. E. G., Wang, X., Burghard, Z., Bill, J., Krasko, A., Boreiko, A., Schloßmacher, U., Schröder, H. C. & Wiens, M. Bio-sintering processes in hexactinellid sponges: fusion of bio-silica in giant basal spicules from Monorhaphis chuni. *J. Struct. Biol.* **168**, 548–561 (2009).
13 Schröder, H. C., Wang, X., Tremel, W., Ushijima, H. & Müller, W. E. G. Biofabrication of biosilica-glass by living organisms. *Nat. Prod. Rep.* **25**, 455–474 (2008).
14 Perry, C. C. & Fraser, M. A. Silica deposition and ultrastructure in cell wall of *Equisetum arvense*: the importance of cell wall structure and flow control in biosilicification? *Philos. Trans. R. Soc. Lond. Ser. B* **334**, 149–157 (1991).
15 Klinowski, J., Cheng, C., Sanz, J., Rojo, J. M. & Mackay, A. L. Structural studies of tabasheer, an opal of plant origin. *Philos. Mag. A* **77**, 201–216 (1998).
16 Ma, J. F. Role of silicon in enhancing the resistance of plants to biotic and abiotic stresses. *Soil Sci. Plant Nutr.* **50**, 11–18 (2004).
17 Soest, P. J. F. Rice straw, the role of silica and treatments to improve quality. *Anim. Feed Sci. Technol.* **130**, 137–171 (2006).
18 Ma, J. F., Tamai, K., Yamaji, N., Mitani, N., Konishi, S., Katsuhara, M., Ishiguro, M., Murata, Y. & Yano, M. A silicon transporter in rice. *Nature* **440**, 688–691 (2006).
19 Currie, H. A. & Perry, C. C. Silica in plants: biological, biochemical and chemical studies. *Ann. Bot.* **100**, 1383–1389 (2007).
20 Epstein, E. Silicon: its manifold roles in plants. *Ann. Appl. Biol.* **155**, 155–160 (2009).
21 Neethirajan, S., Gordon, R. & Wang, L. Potential of silica bodies (phytoliths) for nanotechnology. *Trends Biotechnol.* **27**, 461–467 (2009).
22 Sato, K., Ozaki, N., Nakanishi, K., Sugahara, Y., Oaki, Y., Salinas, C., Herrera, S., Kisailus, D. & Imai, H. Effects of nanostructured biosilica on rice plant mechanics. *RSC Adv.* **7**, 13065–13071 (2017).
23 Kröger, N., Deutzmann, R. & Sumper, M. Silica-precipitating peptides from diatoms—the chemical structure of silaffin-1A from *Cylindrotheca fusiformis*. *J. Biol. Chem.* **276**, 26066–26070 (2001).
24 Shimizu, K., Cha, J., Stucky, G. D. & Morse, D. E. Silicatein alpha: cathepsin L-like protein in sponge biosilica. *Proc. Natl Acad. Sci. USA* **95**, 6234–6238 (1998).
25 Müller, W. E. G., Eckert, C., Kropf, K., Wang, X., Schloßmacher, U., Seckert, C., Wolf, S. E., Tremel, W. & Schröder, H. C. Formation of giant spicules in the deep-sea hexactinellid *Monorhaphis chuni* (Schulze 1904): electron-microscopic and biochemical studies. *Cell Tissue Res.* **329**, 363–378 (2007).
26 Crawford, S. A., Higgins, M. J., Mulvaney, P. & Wetherbee, R. Nanostructure of the diatom frustule as revealed by atomic force and scanning electron microscopy. *J. Phycol.* **37**, 543–554 (2001).
27 Poulsen, N. & Kröger, N. Silica morphogenesis by alternative processing of silaffins in the diatom *Thalassiosira pseudonana*. *J. Biol. Chem.* **279**, 42993–42999 (2004).
28 Mitzutani, T., Nagase, H., Fujiwara, N. & Ogoshi, H. Silicic acid polymerization catalyzed by amines and polyamines. *Bull. Chem. Soc. Jpn* **71**, 2017–2022 (1998).
29 Iler, R. K. *The Chemistry of Silica*, (Wiley, New York, NY, 1979).
30 Zhou, F., Li, S., Vo, C. D., Yuan, J. J., Chai, S., Gao, Q., Armes, S. P., Lu, C. & Cheng, S. Biomimetic deposition of silica templated by a cationic polyamine-containing microgel. *Langmuir* **23**, 9737–9744 (2007).
31 Pi, M., Yang, T., Yuan, J., Fujii, S., Kakigi, Y., Nakamura, Y. & Cheng, S. Biomimetic synthesis of raspberry-like hybrid polymer-silica core-shell nanoparticles by templating colloidal particles with hairy polyamine shell. *Colloids Surf. B* **78**, 193–199 (2010).
32 Hoshino, T., Sato, K., Oaki, Y., Sugawara-Narutaki, A., Shimizu, K., Ozaki, N. & Imai, H. Plant opal-mimetic bunching silica nanoparticles mediated by long-chain polyethyleneimine. *RSC Adv.* **6**, 1301–1306 (2016).
33 Zhao, D., Feng, J., Huo, Q., Melosh, N., Fredrickson, G. H., Chmelka, B. F. & Stucky, G. D. Triblock copolymer syntheses of mesoporous silica with periodic 50 to 300 angstrom pores. *Science* **279**, 548–552 (1998).
34 Yang, P., Deng, T., Zhao, D., Feng, P., Pine, D., Chmelka, B. F., Whitesides, G. M. & Stucky, G. D. Hierarchically ordered oxides. *Science* **282**, 2244–2246 (1998).
35 Nakanishi, K. Pore Structure control of silica gels based on phase separation. *J. Por. Mater.* **4**, 67–112 (1997).
36 Nakanishi, K. & Tanaka, N. Sol-gel with phase separation. Hierarchically porous materials optimized for high-performance liquid chromatography separations. *Acc. Chem. Res.* **40**, 863–873 (2007).
37 Yan, X. & Lei, Z. Silicon dioxide hollow microspheres with porous composite structure: Synthesis and characterization. *J. Colloid Interface Sci.* **362**, 253–260 (2011).
38 Tamaki, R., Naka, K. & Chujo, Y. Synthesis of polystyrene/silica gel polymer hybrids by *in-situ* polymerization method. *Polym. Bull.* **39**, 303–310 (1997).
39 Tamaki, R., Naka, K. & Chujo, Y. Synthesis of poly(*N,N*-dimethylacrylamide) silica gel polymer hybrids by *in situ* polymerization method. *Polym. J.* **30**, 60–65 (1998).
40 Oliver, W. & Pharr, G. Measurement of hardness and elastic modulus by instrumented indentation: advances in understanding and refinements to methodology. *J. Mater. Res.* **19**, 3–20 (2004).
41 Jauffrès, D., Yacou, C., Verdier, M., Dendievel, R. & Ayral, A. Mechanical properties of hierarchical porous silica thin films: experimental characterization by nanoindentation and Finite Element modeling. *Micropor. Mesopor. Mater.* **140**, 120–129 (2011).

Supplementary Information accompanies the paper on Polymer Journal website (http://www.nature.com/pj)